Egypt. J. Chem. **Vol. 66**, No. 7pp. 451 - 464 (2023)

Egyptian Journal of Chemistry

http://ejchem.journals.ekb.eg/

The Synergistic Effect of Graphene / Carboxymethyl Cellulose/ Hydroxyapatite Nanocomposite on Controlled Drug Delivery

Othmane Khalifi Taghzouti, [a] Meriame Bricha, [a] Khalid Nouneh, [b] Anbalagan Ballamurugan, [c] and Khalil El Mabrouk [a,*]

[a] *Euromed Research Center, Euromed University of Fes, Eco-Campus, Meknes Road, 30 300, Fes, Morocco*

[b] *Laboratory of Physics of Condensed Matter (LPMC), Department of Physics, Ibn Tofail University, Kenitra, Morocco*

[c] *Nanobiomaterials & Tissue Engineering Laboratory, Department of Nanoscience and Technology, Bharathiar University, Coimbatore-641 046, Tamil Nadu, India*

Abstract

A new preparation method was reported to synthesize graphene GO - carboxymethyl cellulose CMC and hydroxyapatite HA (GO/CMC/HA). This new bio-nanocomposite was studied to control the loading and release cycle of amoxicillin drugs. The drug loading kinetics and release were studied with respect to the concentration of CMC of the drug carrier while keeping the concentration of GO and HA constant. The targeted delivery of amoxicillin was aimed at using these ternary nanocomposites. The evidence of functional groups and phase purity was analyzed using FTIR spectroscopy and X-ray diffraction techniques. The morphological features were studied using scanning electron microscopy. The thermal property of the developed materials was evaluated by thermogravimetric analysis (TGA). The elastic and storage modulus (G' and G'') as well as the complex viscosity (η*) were recorded for the various concentration of CMC through rheological measurements. The efficiency of the drug delivery was studied using a diffusion mechanism. All the physio-chemical characterizations and rheological studies showed the efficacious synthesis of the new bio- nanocomposites GO/CMC/HA, through in situ precipitation and presents a good candidate to control the drug release applications.

Keywords: Carboxymethyl cellulose; Hydroxyapatite; Graphene oxide; drug delivery; Rheological measurements.

1. Introduction

In recent years, 2D materials have attracted electronics and biomedical research due to their cost-effectiveness and unique properties in a particular structure and extraordinary electronic and mechanical properties [1]. Graphene (GP) is helpful in a wide range of applications, typically in drug delivery systems, high-frequency transistors, solar cells, electrodes in batteries, or as filler in nanocomposites matrix [2]. However, graphene is like carbon nanotubes; their processing and dispersion manipulations present a real challenge to the scientific community by their ability to agglomerate due to the inherent presence of intrinsic Van Der Walls interactions and π-π stacking between layers of graphene [3]. This character limited its use in the biomedical field. Chemical functionalization is a

*Corresponding author e-mail: k.elmabrouk@ueuromed.org.; (Khalil El Mabrouk).
EJCHEM use only: Received date 23 December 2021; revised date 19 February 2022; accepted date 10 March 2022
DOI: 10.21608/EJCHEM.2022.112368.5111

feasible and effective way of improving the dispersion of graphene materials and enhancing the interfacial bonding between the graphene and the matrix. The first and the most used method is oxidation-exfoliation by acid treatment. It confers graphene layers with abundant hydroxyl, epoxide, and carboxylic groups, leading to good graphene oxide (GO) dispersion in a water medium [4]. Up to date, the research has proved that graphene oxide addition could enhance relatively the mechanical properties of GO-related composites. Using a simple self-assembly method, Yang et al. prepared biopolymer nanocomposites from chitosan as a matrix and graphene oxide as a nano-filler [5]. They showed that the incorporation of only 1 wt. % of GO increase the Young modulus and the tensile strength intensively by 64 and 122 %, respectively. Besides, *in vitro* cell studies demonstrated that GO particles significantly increased human mesenchymal stem cell proliferation and bacterial cell apoptosis [6]. Graphene oxide is characterized by a large specific surface area of approximately 2630 m^2/g and high surface energy, which is a primordial factor applied in the bio-composite carrier for medical drugs, especially for many molecules susceptible to environmental variation [7]. GO was also used in drug delivery systems and tissue engineering [8,9].

Furthermore, to develop an ideal interface for biomimetic mineralization and exceed the aggregation in an aqueous solution, the most used method explores the benefit of organic/inorganic composite that can perfectly mimic the bone nature [10].

Chemical functionalization of GO by polysaccharides is the best solution to stabilize GO in an aqueous solution [11]. Polysaccharides have also received significant interest in the same trend, especially for drug delivery applications [12], or paper production and board, according to Y. Fahmy et al. studies [13]. Besides, polysaccharides are used widely as a natural biomaterial to prepare various composites, control the drug release rate and reduce the toxicity effect in the case of fast drug release [14,15]. In the field of biomaterials and tissue engineering applications, polysaccharides are employed, like chitosan [16], heparin [17], pectins [18], dextrans [19], and cellulose [20]. Bao et al. reported the use of chitosan for covalent functionalization of graphene oxide as a nanocarrier to release a water-insoluble anticancer drug "camptothecin, (CPT)," via π- π stacking and hydrophobic interactions [20]. They demonstrated that GO / CS retains a high-efficiency loading of CPT near 20 wt. %. An *in-vitro* drug release experiment indicated that 18 wt.% of CPT was released upon 72h at 37 °C in PBS buffer solution [10]. Joung. et al. prepared a new self-assembling heparin-pluronic nano-gel able to release multi-therapeutic agents and thus improve the healing efficiency of the cancer chemotherapy blend [17]. Another research studied the crosslinking of nano-gel based on hydroxypropyl cellulose and displayed a rapid drug release around tumor cells [20].

Carboxymethyl cellulose (CMC) is the most important cellulose derived, primarily used in pharmaceutics, especially for proteins and drug release among these polysaccharides. Furthermore, a great interest was focused on CMC as 3D scaffolds for tissue engineering. However, many efforts are required to achieve this goal [21]. Carboxymethyl cellulose is a natural biodegradable biopolymer characterized by good solubility, high chemical stability, non-toxic, safe, biocompatible, and hydrophilic. Furthermore, carboxylate and hydroxyl groups Form the CMC to exert strong interaction with drug molecules. Therefore, they have a potential range of applications as aimed drug delivery systems in the biomedical field [22], wastewater treatment, antimicrobial activity and polymer nanocomposites production [23–26]. More recently, CMC has been used to stabilize graphene oxide sheets, owing to the functional groups (carboxylic and hydroxyl groups), resulting in non-covalent solid interaction between CMC and GO. However, no detailed study has been conducted until now in studying the effect of varying CMC concentrations on the dispersion and stabilization of graphene oxide sheets and the subsequent use of the prepared composites in the adsorption and release of bioactive molecules.

Hydroxyapatite (Ca_{10} $(PO_4)_6OH_2$, (HA)) is the primary inorganic compound of natural bone that has been studied extensively in bone tissue regeneration due to its biocompatibility, osteoinduction, and osteoconduction. HA is a bioactive material capable of creating a new bone via chemical interactions with adjacent tissue without causing any immune reactions in the human body. Further, HA has been used in

various applications such as drug delivery and anticancer [27], anti-inflammatory [28], and anti-osteoporotic [29]. However, the fact that hydroxyapatite has a brittle character limits its use. This allows developing materials in other forms as a new class of polymer-hydroxyapatite composites and nano-composites. Since natural bone is comparable to a nanocomposite comprising HA nanoparticles of uniform morphology (shape, size), with crystallographic orientation grown and hierarchically impregnated in a collagen matrix. Similar to a biomimetic process, it has been developed to *in situ* synthesize HA in a bio-polymeric matrix [30]. In recent years, several studies reported the growth of HA particles on GO layers in a bio-mineralization medium, in which GO was functionalized by polysaccharides such as gelatin [31], carrageen [32], chitosan [33]. According to these works, it was found that bio-mineralization took a long period of immersion of about 14 to 21 days. For loading/release drug applications, hydroxyapatite is not an excellent candidate to meet this demand because of the weak interaction between HA and drug molecules. Therefore, the behavior during drug release became significantly faster [34]. Recently, M. Ahangari et al. synthesized a new composite based on hydroxyapatite, carboxymethyl cellulose, and graphene. However, they investigated the use of the produced composite as a coating on AZ31 magnesium alloy through the electrophoretic deposition method. They found that graphene and carboxymethyl cellulose enhance the elastic modulus and the adhesion on the coating, respectively [35].

Nowadays, real progress is concentrated on composites-based graphene. However, there is no report on GO/CMC/HA composites as a template for drug delivery systems. This work reports a non-time-consuming technique to prepare GO/CMC/HA hybrid materials, with various amounts of CMC concentrations, through *in situ* precipitation method. Present work also reported the effect of CMC addition on the physico-chemical behaviour of synthesized hydroxyapatite nanoparticles. In addition, it investigates drug storage/release kinetic in synthetic body fluid solution (SBF) using amoxicillin as a model drug molecule.

2. Experimental

2.1. Materials

Natural graphite, sodium carboxymethyl cellulose, Amoxicillin ($C_{16}H_{19}N_3O_5S$), sulphuric acid (H_2SO_4), sodium nitrate ($NaNO_3$), potassium permanganate ($KMNO_4$), hydrogen peroxide (H_2O_2), Hydrochloric acid (HCl), calcium chloride ($CaCl_2$), ammonia solution (NH_3), phosphoric acid (H_3PO_4) were purchased from Sigma Aldrich Chemicals, with high purity grade. The starting precursors are used without any purification.

2.2. Preparation of graphene oxide (GO)

Graphene oxide (GO) was synthesized using Hummer's method from natural graphite [36]. Briefly, 2g of graphite powder and 1 g of $NaNO_3$ were added to 50 mL of concentrated H_2SO_4 and were stirred in an ice bath, and then 6g of $KMnO_4$ was slowly added with vigorous stirring. Next, the suspension was kept at 35°C for 30 min with stirring. After this step, 180 mL of distilled water was added to the solution, treated at 95°C, and stirred for 30 min. Then, 450 mL of distilled water was slowly added, followed by 15 mL of H_2O_2 (30%). Finally, the resulting mixture was filtered via a Millipore membrane filter with a pore diameter of 0.2 µm under vacuum and then washed thoroughly with distilled water after HCl (1M, 37%) until the suspension was neutral dried at 60°C for 24h.

2.3. Preparation of graphene oxide /carboxymethyl cellulose composites

As detailed in Table 1, a Predetermined amount of CMC was dissolved in 50 mL of distilled water and stirred mechanically at 45 rpm for 1h at 45 °C. Next, a predetermined amount of graphene oxide was dispersed by ultra-sonication on 50 mL of distilled water for 2h; CMC solution was added to GO solution and dispersed for an additional 30 min by ultra-sonication.

Table 1

Weight % of CMC used in the composite system (the HA/GO is constant)

Samples acronym	wt.% (HA)	wt. % (GO)	wt. % (CMC)
GO/CMC/HA (a)	81.5609	2.4468	15.9923
GO/CMC/HA (b)	65.7810	1.9734	32.2456
GO/CMC/HA (c)	49.7415	1.4922	48.7662
GO/CMC/HA (d)	39.9906	1.1997	58.8097
GO/CMC/HA (e)	33.4360	1.0031	65.5609
Samples acronym	wt.% (HA)	wt. % (GO)	wt. % (CMC)

2.4. Preparation of graphene oxide / Carboxymethyl cellulose / hydroxyapatite (GO/CMC/HA) composites

As illustrated in scheme 1, Hydroxyapatite was precipitated in the presence of GO and GO-CMC matrix at a relatively different weight fraction of CMC through the in-situ precipitation method. For all samples, the GO/HA percentage ratio is maintained at 3 wt. % relative to the theoretically synthesized weight of HA. $CaCl_2$ precursors (10.25 mM) were dissolved in 50 mL of distilled water, and the solution was added dropwise to CMC-GO solution under stirring. After that, 50 mL of diluted H_3PO_4 (6.14 mM) was added to the previous solution under agitation (45 rpm) for 30 min. The pH of the solution was then adjusted to 10 by adding an ammonia solution (NH_3). The solution was then stirred for 24h at 37°C. The resulting precipitate was centrifuged and washed four times with distilled water and ethanol. The obtained powder was dried at 80 ºC overnight.

Different GO/CMC/HA composites with a varied amount of CMC (Table. 1) were elaborated via the *in-situ*-precipitation method, as illustrated in Scheme1. First, GO was ultra-sonicated to initiate graphene oxide sheets' exfoliation and to form a stable aqueous suspension. Then, CMC was used to functionalize GO under the same conditions to enhance the dispersion quality of GO/CMC composites. During the synthesis of hydroxyapatite by in situ precipitation, polar functional groups of GO/CMC composites on the surface act as nucleation and growth sites of HA particles. Then, the calcium ions (Ca^{2+}) are added to bond to the remaining functions, such as epoxy, hydroxyl, carboxylic functional groups of GO/CMC composites via electrostatic interaction, and lead to a positively charged layer. Then, this latter attracts phosphate ions (PO_4^{3-}). Finally, the nucleation and growth of hydroxyapatite nuclei occur on GO/CMC surface to become crystals of HA for prolonged periods.

2.5. Physico-chemical characterizations

Fourier transform infrared (FTIR) analyses were carried out on a Thermoscientific, IS-50 FT-IR in the frequency range of 4000 - 400 cm^{-1} to identify the functional groups of the composites, with 4 cm^{-1} as resolution. The X-ray diffraction (XRD) patterns of the powders and composites were assayed using an automated X-ray powder diffractometer (XRD, PANalytical) at a scanning rate of 0.033° per second in a 2θ range from 20° to 80° with Cu-Kα radiation (λ = 1.54060 Å), operated at 45 kV and 40 mA. Thermogravimetric analysis (TGA) was conducted with TGA Q500. All the samples were carefully grounded to a fine powder. The samples were analysed within the temperature range 25-1000 °C at a 10 °C / min heating rate under the atmospheric environment. The morphology and elemental analysis of nanocomposites were carried out using scanning electron microscopy (SEM) on FEI Quanta 200 EDAXR. CMC solutions with different weight fractions similar to those used to serve hybrid composites were prepared under mechanical stirring. In coaxial cylinder geometry, rheological measurements were carried out on the MCR501 constant strain Rheometer from Anton Paar-Physica. Steady-state measurements were achieved between 0,1 to 100 s^{-1}, and frequency sweep tests under small-amplitude oscillatory shear flow (SAOS) at room temperature were measured from low to high values. The elastic and storage modulus (G' and G'') as well as the complex viscosity (η*) were recorded for the various concentration of CMC. The gel structure will be defined when the plateau modulus slope decreases dramatically to reach values lower than $< < 1$ in the case of G'', and when viscosity is raised to higher values in steady-state measurements.

2.6. Amoxicillin loading and release on GO/CMC/HA composites

GO/CMC/HA nanocomposites with different amounts of CMC were dispersed in an aqueous solution using sonication with 0.8 frequency and an amplitude of 80%. The amoxicillin was added to nanocomposites solutions and kept for 24h at 37°C under a dark environment. The mass ratio of AMX to the composite matrix is fixed to 1 mg/1 ml. After that, the solution was centrifuged at 10000 rpm for 5 min, and the drug loading was calculated according to equation (1). Each experiment was triplicated to get the mean and the standard deviation.

The release of AMX from various nanocomposite samples (GO/CMC/HA) was carried out by dispersing pre-weighed samples in PBS medium at pH = 7.42 and 37°C relatively to multiple periods of times (1, 2,

4.5, 5.5, 24, 48, 72 and 96h). 4 mL of dissolution medium was collected at a predetermined time, and the same volume was replaced. The PBS solution was analysed at 272 nm by UV/VIS Spectrometer Lamda-850. The experiments were repeated three times to get the mean and the standard deviation. The amount of the AMX released was calculated using linear regression analysis. The cumulative release of AMX was calculated from equation (2):

$$\text{Drug loading (\%)} = \frac{m_0 - m_t}{m_0} \times 100 \qquad \text{Eq. 1}$$

$$\text{Cumulative drug release (\%)}_t = \left(\frac{m_t}{m_0} \times 100\right)_t + (\text{\% drug release})_{t-1} \qquad \text{Eq.2}$$

Where: m_0 is the initial mass of drug used in loading (1mg/ml), m_t is the mass of AMX collected in aqueous or PBS solution, and t is the time of collection.

3. Results and discussion

3.1. FTIR analysis of GO and GO/CMC/HA nanocomposites

Hummers' method was used to prepare GO with good purity. The preparation of graphene under its oxidized form is essential to reduce the cytotoxicity effect of carbonaceous nanomaterials [6]. FTIR spectroscopy (Fourier transform infrared spectroscopy) confirms the successful preparation of GO, as shown in Fig. 1. The FTIR spectrum of GO exhibits oxygen processing groups at 3203, 1730, 1620, 1246, and 1051 cm^{-1}. These bands are correlated to hydroxyl groups (O-H), carboxyl group C=O, sp2-hybridized C=C stretching vibration, C-OH stretching vibration, and epoxy C-O groups on the surface of GO [37]. Fig. (1B) showed the characteristics absorption bands of CMC at 1590, 1415, 1329, and 1026 cm^{-1} and were assigned to C=O vibration, C-H vibration of CH_2, and carboxymethyl ether group stretching, respectively [38,39]. Fig. (1B) also displays the infrared spectra of HA synthesized by precipitation method as a reference without any template. It confirms the prominent vibration of phosphate groups at 478, 564, 962-1088 cm^{-1}, and a large band at around 3200-3500 cm^{-1} revealed the presence of absorbed water, characteristics bands of hydroxyapatite phase [40].

According to Fig. (1B (a-e)), it was remarked no change in the spectra of nanocomposites as a function of CMC concentration if compared with GO/HA composites, except for compositions with a high amount of CMC (Fig. 1B c, d, and e). As the polysaccharide concentration is minimal, it was insufficient to prevent hydroxyapatite particles-growth on GO surfaces. Once the amount of CMC increased, more interactions between CMC and GO could be achieved. The system is evolved toward viscous media that prevent less diffusion of chemical entities responsible for hydroxyapatite formation. This was also confirmed by the apparition of new characteristics bands at 556, 600, 1016, 1088, and 3307 $cm^{-1,}$ respectively. The carboxyl groups of C=O at 1730 cm^{-1}) disappeared entirely in the composites. This may be referred to as the interaction between the carboxylic groups of GO/CMC [41]. SEM observations and rheological measurements will support more explanations.

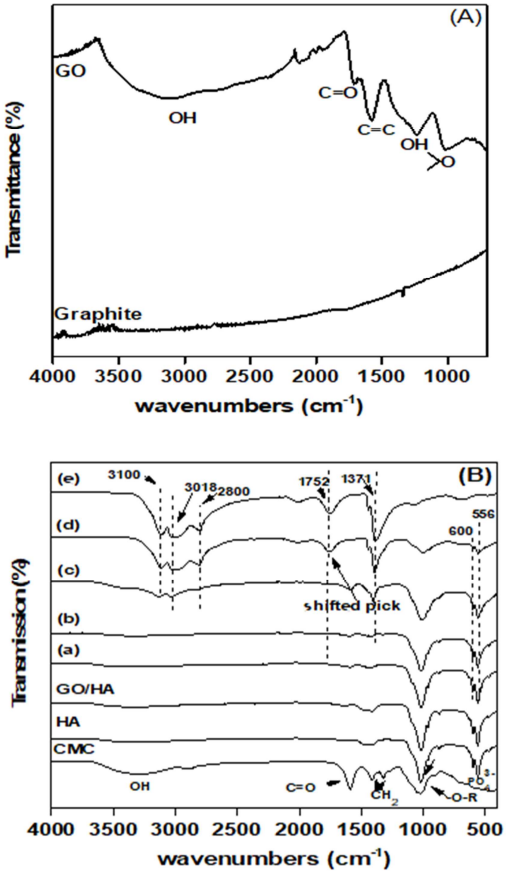

Fig. 1: FTIR spectra of (A) graphite and graphene oxide, (B) GO/CMC/HA corresponding nanocomposites

3.2. X-ray diffraction characterization (XRD)

The X-ray diffraction characterization was accomplished to analyse phase composition and to demonstrate the crystallinity of the prepared HA, GO/HA, and GO/CMC/HA nanocomposites. Fig. 2A showed the XRD patterns of graphite (GP) and graphene oxide (GO). Graphite flakes displayed an intense diffraction peak, 26.5°θ, related to the (001) lattice plane. On the other hand, after the oxidation, GO flakes showed a diffraction peak at 2θ = 10.1°θ and corresponded to (002) reflection. The decrease of 2θ from GP to GO is closely related to the increase of *d* spacing after oxidation. This increment in *d* spacing is attributed to a rise in the interlayer distance of oxidized graphite due to functional groups on the GO surface. These results confirm the successful introduction of hydroxyl, epoxy, and carboxyl groups between graphite layers and the preparation of GO flakes [6,32,42].

According to Fig. 2B, the prominent peaks of HA were observed at 26, 31.8, 32.86, 46, 53,36 °θ, which could be corresponded to (002), (211), (300), (222), and (004) lattice planes of the hexagonal HA, respectively. They all show a good resemblance with the standard JCPDS file [JCPDS #09-0432], meaning that the powders consist of an apatitic phase [43,44]. The XRD pattern of GO/HA shows the same typical diffraction peaks as the hydroxyapatite phase. According to Fig. 2B (a-e), predominant peaks of the hydroxyapatite phase were observed. As known, that CMC has a broad diffraction peak at 20.52°θ [45]. However, in the present study, nanocomposite samples with a high amount of polysaccharides (from 0.5 wt % of added CMC to 1 wt %.) presented slight changes. The apparition of a new diffraction peak around 22.83°θ, which belongs to the CMC phase with a bit of shift, indicating the apparent functionalization of GO by CMC, due to the hydrogen bonding electrostatic interaction. It is noticed that the XRD spectrum peaks of the nanocomposites became narrower as a function of CMC addition, indicating the enhancement of the crystallinity degree of HA.

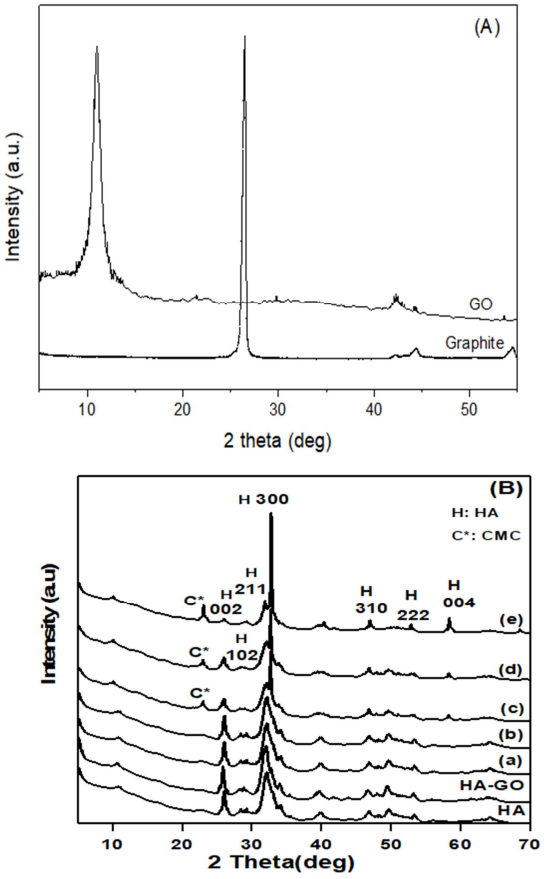

Fig. 2: (A) XRD patterns of Graphite (Gr) and graphene oxide (GO), (B) XRD patterns of GO/CMC/HA

3.3. Thermogravimetric analysis (TGA)

The thermal stability of GO, HA, GO/HA, and GO/CMC/HA were studied by a TGA analyser in the temperature range from ambient to1000°C under an atmospheric environment. The results are summarized in Fig. 3. The TG curves of GO and CMC (Fig. 3A) indicated that these materials are both thermally unstable. The initial weight loss of all samples was recorded at around 150°C. It was attributed to the evaporation of adsorbed water. The weight loss is between 5 to 11 % for hydroxyapatite and GO/CMC/HA (c) nanocomposite, respectively. For GO, the weight loss occurred at three different stages, namely (i) up to 150 °C, (ii) between 150-250 °C, and (iii) 250-900 °C. The second drop was found to be about 40 wt. %, and could be attributed to the evaporation of interlamellar water and decomposition of labile oxygen. The weight loss at the later stage is very consistent with a value of 59 wt.%, which represents the carbon combustion composing GO

sheets [46,47]. However, for CMC, the degradation rate was very fast as also reported by Liu et al. [48] From Fig. 3A, we detected five steps of total weight loss, ascribed as follows: (i) up to 150°C, (ii) 150-200°C, (iii) 200-530 °C, (iv) 530-650 °C and (v) 650-900 °C. In the range of 200-530 °C, a dramatic drop of weight loss occurred (55 wt. %) and continued to decrease until 900 °C. Finally, the global weight loss reached a value of 82 wt. % above 900°C.This behaviour is explained by the loss of carboxyl anion (COO^-) groups from the polysaccharide at the beginning, followed by the total degradation of the remaining material into carbon residues [49,50].

The thermal analysis of HA, GO/HA, and GO/CMC/HA nanocomposites are illustrated in Fig. 3B. The thermal degradation of pure HA can be divided into three mean regions. The weight loss between room temperature to 200°C is mainly attributed to the evaporation of physically absorbed water. Within the 200-600 °C range, the weight loss corresponded to the decomposition reactions of the unreacted precursor's reagents. In the last stage (600-1000 °C), small and slow decompositions occur until reaching a steady state around a total weight loss of 8 wt.%, which explains the stability of the HA phase [51]. In the case of GO/HA, a slight difference concerning the total weight loss was recorded to be around 10 wt. %, in reasonable agreement with the fixed rate of GO/HA equal to 3 wt. % according to all synthesized samples. Concerning samples with CMC content, it can be seen that the total weight loss gradually increases with increasing the added amount of CMC, ranging from 10 wt. % in the case of GO/HA, to 64 wt. % for samples containing the highest amount of CMC (e). It should be also noted that for the compositions (a, b), the thermal decomposition of the nanocomposites remains moderate for the low concentration of CMC. However, for samples with high CMC content, it was observed that the degradation is much more pronounced, and it increased with CMC concentration.

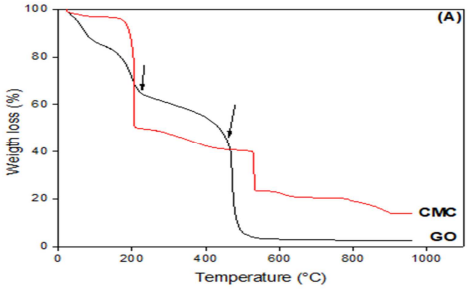

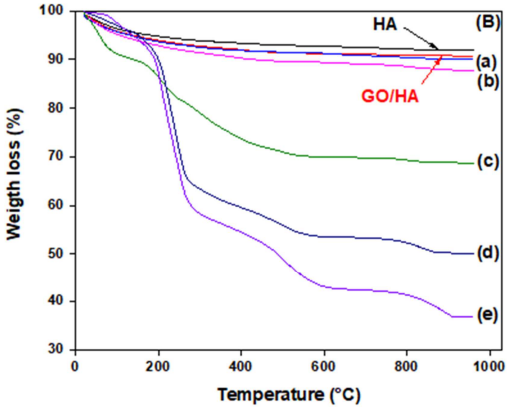

Fig. 3: TGA profiles of GO, CMC (A), and pure HA, GO/HA, GO/CMC/HA (a, b, c, d, e) (B)

Rheological studies versus morphological characterization

From a rheological point of view (Fig. 4), it was noticed that the viscosity behaviour of the prepared samples is CMC's concentration-dependent. For lower concentrations of CMC (Fig. 4a', b' and c'), the viscosity remains constant doesn't matter the applied shear rates. In contrast, the viscosity recorded a lower value for a sample with 15 wt.% of CMC (Fig. 4a') and increased with increasing the concentration from a' to c'. According to these samples, the Newtonian viscosity behavior confirmed well that there is no change in the molecular structures. However, once the concentration of CMC reaches 58 %, a shoulder at a lower shear rate is recorded (Fig. 4d' and e'), whereas a shear-thinning is observed at high shear rates. These observations confirm well the gel formation for both samples. SEM observations confirm these results.

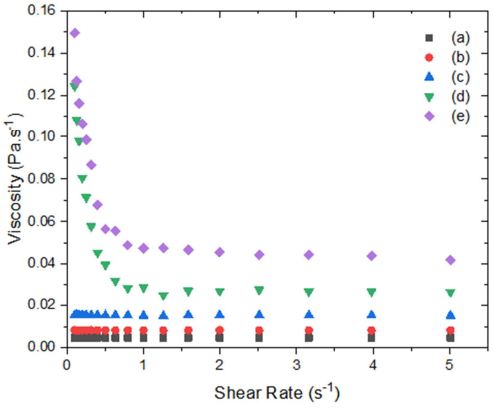

Fig. 4: The flow behavior of GO/CMC blend as a function of CMC concentration before HA *in-situ* precipitation

According to Fig. 5, the SEM micrographs revealed that the GO displayed sheet-like

morphology. It consists of thin, randomly crumpled sheets. The same observations were raised by Turk et al. [52], and Sumathra et al. [42]. For composites materials with CMC, one can observe a noticeable change in the morphology of the GO sheets, as shown in Fig. 4 (b'-d'). Only nanocomposites ***a***, ***d*** and ***e*** are presented since the nanocomposites ***a***, ***b*** and ***c*** have almost the same behaviour, as discussed in the previous characterizations. From Fig. 4 (b'), which show surface SEM micrograph of GO/CMC/HA (a), we remark dense layers of hydroxyapatite particles on the surface of GO/CMC matrix, with small irregular globular morphology, leading significantly to the alteration of the surface topography of GO.

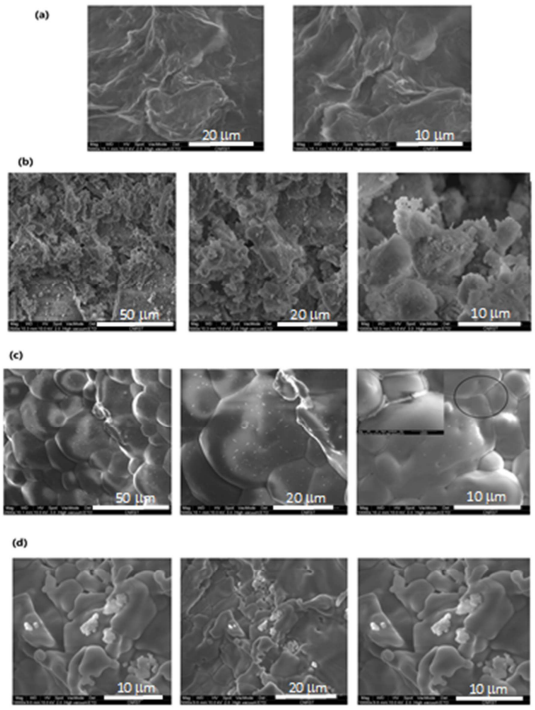

Fig. 5: SEM micrographs of (a) GO sheets, (b) GO/CMC/HA (a), (c) GO/CMC/HA (d), (d) GO/CMC/HA

Even with low percentages, the simultaneous presence of GO and CMC leads to preferential nucleation and the growth of the crystalline hydroxyapatite phase. This was mainly attributed to the total exfoliation of GO nano-sheets after the incorporation of CMC, which contributed to the bird of strong interfacial bonding for the as-formed HA nanoparticles. In a recent study, Chen et al. proposed an effective route to functionalize GO with biologically HA through *in situ* synthesis at low temperatures. They concluded that hydroxyapatite crystalline is preferentially nucleated at GO surfaces to highly crystalline HA nanowhiskers [7]. The incorporation of a high amount of CMC to GO effectively changed the surface topography of GO, leading to a smooth surface, which indicates the homogeneous dispersion of GO nano-sheets by CMC due to the electrostatic interaction (Fig. 4 (c'-d')).

Furthermore, at this level of CMC, our matrix changes to a gel foam, and hydroxyapatite crystallize in and between GO/CMC sheets, as observed in Fig. 4 (c' – d'). The HA nanoparticle migration to the edges of nanocomposites is mainly attributed to the strong interactions between the abundant hydroxyl, epoxide, and carboxylic groups on the basal plane and edges of GO/CMC nanocomposites and HA nanoparticles, respectively. Thus, we can conclude that GO/CMC supports hydroxyapatite particle nucleation and growth. Furthermore, CMC weight fraction variation affects the quality of GO sheet exfoliation and the morphology of precipitated HA nanoparticles homogeneously.

3.4. AMX loading and in vitro drug release

To evaluate the loading and releasing property of nanocomposite materials, the water-soluble antimicrobial drug Amoxicillin was selected as a model drug. The calibration curve for the various concentration of AMX was realized and traced (Fig. 6).

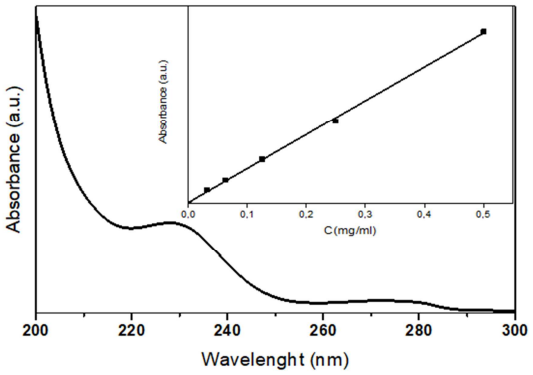

Fig. 6: UV-vis spectrum of pure AMX (the inset represents curve calibration)

Fig. 7A shows the loading of amoxicillin molecules with GO, HA, and GO/CMC/HA nanocomposites. It can be seen that graphene oxide exhibited an extremely high loading efficiency of amoxicillin with a percentage of 82.19 compared to pure HA with a value of 51.99 %. This result is mainly ascribed to the high specific area of GO. At the same time, GO can form π-π stacking interaction between hydroxyl and carboxylic groups on the GO sheet from one side and amino, hydroxyl, and sulphur groups of AMX from the other side [53]. It is noticed that GO/CMC/HA nanocomposites and the drug's adsorption are strongly dependent on the weight fraction of CMC added. GO/CMC/HA (a) has a loading efficiency of about 41.04 %, slightly lower than pure HA. This diminution is explained by a slight decrease of functional groups by CMC molecules on the surface of graphene oxide, which reduces the capacity of the nanocomposites to absorb more drug molecules.

From the same figure (Fig. 7), it was proved that the increase of CMC content from sample *a* to *e* nanocomposite induced an enhancement of amoxicillin loading efficiency, reaching the highest value of 77, 45 %. These results are in total agreement with previous reports [54,55].

Fig. 7B shows the drug release profile of AMX drug molecules in PBS medium for HA, GO, GO-HA, GO/CMC/HA (a, b, c, d, and e). According to this figure, the drug-release profiles of all nanocomposites are proportional to the time release. In fact, the release profile is characterized by a fast issue up to the first 5h after it reached an equilibrium statute. It is observed that the cumulative drug release is closely dependent on the amount of carboxymethyl cellulose in nanocomposite materials. Hence, nanocomposites can be introduced as suitable candidates for target drug delivery systems with controlled release. As a result, CMC prevents AMX from fast release, leading to a high drug concentration in the biomaterial and, consequently, procuring cell toxicity for the patient [56]. The prepared nanocomposites GO/CMC/HA (d, e) have an excellent performance than other prepared biomaterials. Consequently, these nanocomposites exhibited great potential as a novel carrier for drug delivery and release. Otherwise, the influence of release rate could be explained by either drug diffusion or eroding of CMC, also depending on the polymer characteristic such as molecular weight, hydrophilic-hydrophobic composition, and polydispersity of the nano-aggregates [57].

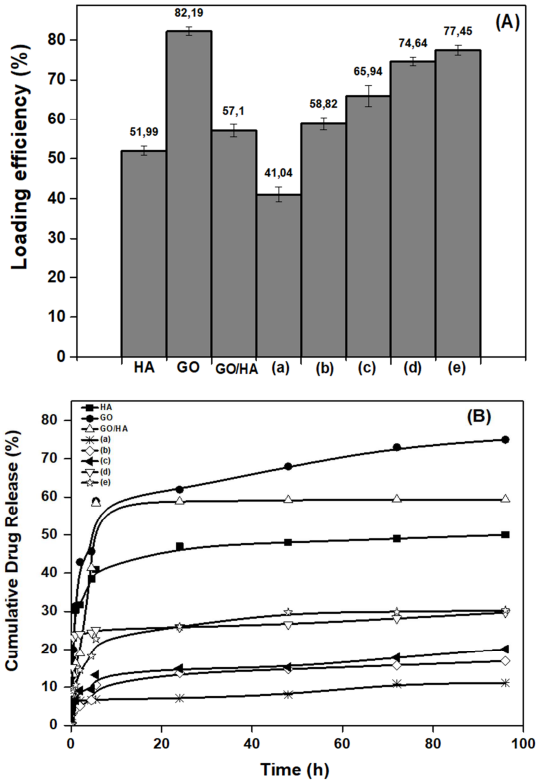

Fig. 7: AMX loading (A) and release (B) profiles from HA, GO, GO/HA and GO/CMC/HA carriers

In order to identify the mechanism that governs the release of AMX from all samples. A semi-empirical model was developed by Ritger & Peppas (Eq. 3) [58], and kopcha (Eq. 4) [59] [60], a simple equation was proposed to describe the release behaviour of controlled release drug and to quantify the contribution of diffusion and erosion :

$$\frac{M_t}{M_\infty} = kt^n \qquad \text{Eq. 3}$$

$$M_t = A\sqrt{t} + Bt \qquad \text{Eq. 4}$$

$\frac{M_t}{M_\infty}$ Is the fractional solute release, M_t is the amount of released drug at time t, M_∞ is the total amount of released drug, k is a constant, and n is the diffusional exponent characteristic of the release mechanism. n provide more information about the drug-release mechanism. If n < 0.5, the mechanism

corresponds to Fickian diffusion, and if n is located between 0.5 and 1.0, the mechanism corresponds to non-Fickian transport.

For equation 4, A is a diffusional term, and B is the erosion term. When A/B >1, the diffusion phenomenon is predominant, and when A/B <1, the erosion phenomenon is predominant. Table 2 shows the parameter calculation results of n, A, and B, respectively. According to the calculated factors, it can be determined from both models that the drug molecules' release followed the Fickian diffusion law for all samples.

Table 2

Parameters of the AMX release profile fitting according to Ritger & Peppas and Korsmeyer models

Samples	Korsmeyer–Peppas	Kopcha
	n	A/B
HA	0,39	>>1
GO	0,38	>>1
GO/HA	0,32	>>1
GO/CMC/HA (a)	0,22	>>1
GO/CMC/HA (b)	0,37	>>1
GO/CMC/HA (c)	0,36	>>1
GO/CMC/HA (d)	0,28	>>1
GO/CMC/HA (e)	0,32	>>1

4. Conclusions

In summary, in this paper, a new hybrid composites based on graphene oxide/carboxymethyl cellulose/ hydroxyapatite as a matrix (GO/CMC/HA), was successfully synthesized through *in situ* precipitation. After nucleation and growth of HA, the obtained results suggest that the loading and release capacity of GO/CMC/HA was controlled by CMC content in the composite. The loading and release of amoxicillin (AMX) drug from composite increase with the increase of the weight fraction of CMC, and the AMX loading and release becomes more controllable with the increases of composite stability. Furthermore, the analysis about the drug release showed that a diffusion mechanism controlled all samples' amoxicillin release mechanism. According to the results, the composite may benefit controlled drug release applications.

5. Conflicts of interest

The authors declare there is no conflict of interest.

6. Formatting of funding sources

This work is a part of the financial support allowable from the Euromed University of Fes - Morocco and National Center for Scientific and Technical Research – Morocco, PPR2 Program.

7. Acknowledgments

The authors are grateful for the financial support from the Euromed University of Fes - Morocco and the National Center for Scientific and Technical Research – Morocco, PPR2 Program.

8. Authors contribution

OKT, KEM and MB conceived and planned the project, the experiments' main conceptual ideas, and design. OKT implemented the experiments. OKT, KEM, and MB contributed to data analysis and interpretation of the results. OKT was in charge of writing the first draft. KEM and MB contributed to writing and also reviewing the final version of the manuscript. All authors provided helpful feedback.

9. References

[1] Kumar, S., and Chatterjee, K. Comprehensive Review on the Use of Graphene-Based Substrates for Regenerative Medicine and Biomedical Devices. *ACS Applied Materials and Interfaces*, 8 (40), 26431–26457 (2016).

[2] Barwich, S., Khan, U., and Coleman, J.N. Article A Technique to Pre-Treat Graphite Which Allows the Rapid Dispersion of Defect-Free Graphene in Solvents at High Concentration A Technique to Pre-Treat Graphite Which Allows the Rapid Dispersion of Defect-Free Graphene in Solvents at High Concentra. (2013).

[3] Bricha, M., and Mabrouk, K. El PT SC. *Colloids and Surfaces A: Physicochemical and Engineering Aspects* (2018).

[4] Zhu, J. Monolayers with an IQ. 3 (September) (2008).

[5] Yang, X., Tu, Y., Li, L., Shang, S., and Tao, X. Well-Dispersed Chitosan/Graphene Oxide Nanocomposites. 2 (6), 1707–1713 (2010).

[6] Kumar, S., Raj, S., Kolanthai, E., Sood, A.K., Sampath, S., and Chatterjee, K.

Chemical functionalization of graphene to augment stem cell osteogenesis and inhibit biofilm formation on polymer composites for orthopedic applications. *ACS Applied Materials and Interfaces*, 7 (5), 3237–3252 (2015).

[7] Chen, C., Sun, X., Pan, W., Hou, Y., Liu, R., Jiang, X., and Zhang, L. Graphene Oxide-Templated Synthesis of Hydroxyapatite Nanowhiskers to Improve the Mechanical and Osteoblastic Performance of Poly(lactic acid) for Bone Tissue Regeneration. *ACS Sustainable Chemistry and Engineering*, 6 (3), 3862–3869 (2018).

[8] Justin, R., and Chen, B. Characterisation and drug release performance of biodegradable chitosan–graphene oxide nanocomposites. *Carbohydrate Polymers*, 103, 70–80 (2014).

[9] Liu, Z., Robinson, J.T., Sun, X., and Dai, H. PEGylated nanographene oxide for delivery of water-insoluble cancer drugs. *Journal of the American Chemical Society*, 130 (33), 10876–10877 (2008).

[10] Bao, H., Pan, Y., Ping, Y., Sahoo, N.G., Wu, T., Li, L., Li, J., and Gan, L.H. Chitosan-functionalized graphene oxide as a nanocarrier for drug and gene delivery. *Small*, 7 (11), 1569–1578 (2011).

[11] Mianehrow, H., Moghadam, M.H.M., Sharif, F., and Mazinani, S. Graphene-oxide stabilization in electrolyte solutions using hydroxyethyl cellulose for drug delivery application. *International Journal of Pharmaceutics*, 484 (1–2), 276–282 (2015).

[12] Liu, Z., Jiao, Y., Wang, Y., Zhou, C., and Zhang, Z. Polysaccharides-based nanoparticles as drug delivery systems. *Advanced Drug Delivery Reviews*, 60 (15), 1650–1662 (2008).

[13] Fahmy, Y., Fahmy, T., Mobarak, F., El-Sakhawy, M., and Fadl, M. Agricultural Residues (Wastes) for Manufacture of Paper, Board, and Miscellaneous Products: Background Overview and Future Prospects. *International Journal of ChemTech Research*, 10 (2), 424–448 (2017).

[14] Chen, S., Liu, M., Jin, S., and Wang, B. Preparation of ionic-crosslinked chitosan-based gel beads and effect of reaction conditions on drug release behaviors. *International Journal of Pharmaceutics*, 349 (1–2), 180–187 (2008).

[15] Şanlı, O., Ay, N., and Işıklan, N. Release characteristics of diclofenac sodium from poly(vinyl alcohol)/sodium alginate and poly(vinyl alcohol)-grafted-poly(acrylamide)/sodium alginate blend beads. *European Journal of Pharmaceutics and Biopharmaceutics*, 65 (2), 204–214 (2007).

[16] Feng, C., Sun, G., Wang, Z., Cheng, X., Park, H., Cha, D., Kong, M., and Chen, X. Transport mechanism of doxorubicin loaded chitosan based nanogels across intestinal epithelium. *European Journal of Pharmaceutics and Biopharmaceutics*, 87 (1), 197–207 (2014).

[17] Joung, Y.K., Jang, J.Y., Choi, J.H., Han, D.K., and Park, K.D. Heparin-conjugated pluronic nanogels as multi-drug nanocarriers for combination chemotherapy. *Molecular Pharmaceutics*, 10 (2), 685–693 (2013).

[18] Zhou, M., Wang, T., Hu, Q., and Luo, Y. Low density lipoprotein/pectin complex nanogels as potential oral delivery vehicles for curcumin. *Food Hydrocolloids*, 57, 20–29 (2016).

[19] Li, D., Kordalivand, N., Fransen, M.F., Ossendorp, F., Raemdonck, K., Vermonden, T., Hennink, W.E., and Van Nostrum, C.F. Reduction-sensitive dextran nanogels aimed for intracellular delivery of antigens. *Advanced Functional Materials*, 25 (20), 2993–3003 (2015).

[20] Rahimian, K., Wen, Y., and Oh, J.K. Redox-responsive cellulose-based thermoresponsive grafted copolymers and in-situ disulfide crosslinked nanogels. *Polymer*, 72, 387–394 (2015).

[21] Juncu, G., Stoica-Guzun, A., Stroescu, M., Isopencu, G., and Jinga, S.I. Drug release kinetics from carboxymethylcellulose-bacterial cellulose composite films. *International Journal of Pharmaceutics*, 510 (2), 485–492 (2016).

[22] Butun, S., Ince, F.G., Erdugan, H., and Sahiner, N. One-step fabrication of biocompatible carboxymethyl cellulose polymeric particles for drug delivery systems. *Carbohydrate Polymers*, 86 (2), 636–643 (2011).

[23] Aldalbahi, A., El-naggar, M., Khattab, T.,

Abdelrahman, M., Rahaman, M., Alrehaili, A., and El-newehy, M. Development of green and sustainable cellulose acetate/graphene oxide nanocomposite films as efficient adsorbents for wastewater treatment. *Polymers*, 12 (11), 1–16 (2020).

[24] Kassab, Z., Boujemaoui, A., Ben Youcef, H., Hajlane, A., Hannache, H., and El Achaby, M. Production of cellulose nanofibrils from alfa fibers and its nanoreinforcement potential in polymer nanocomposites. *Cellulose*, 26 (18), 9567–9581 (2019).

[25] Khattab, T.A., El-Naggar, M.E., Abdelrahman, M.S., Aldalbahi, A., and Hatshan, M.R. Facile development of photochromic cellulose acetate transparent nanocomposite film immobilized with lanthanide-doped pigment: ultraviolet blocking, superhydrophobic, and antimicrobial activity. *Luminescence*, 36 (2), 543–555 (2021).

[26] Vatansever, E., Arslan, D., and Nofar, M. Polylactide cellulose-based nanocomposites. *International Journal of Biological Macromolecules*, 137, 912–938 (2019).

[27] Xiong, H., Du, S., Ni, J., Zhou, J., and Yao, J. Mitochondria and nuclei dual-targeted heterogeneous hydroxyapatite nanoparticles for enhancing therapeutic efficacy of doxorubicin. *Biomaterials*, 94, 70–83 (2016).

[28] Öner, M., Yetiz, E., Ay, E., and Uysal, U. Ibuprofen release from porous hydroxyapatite tablets. *Ceramics International*, 37 (7), 2117–2125 (2011).

[29] Seshima, H., Yoshinari, M., Takemoto, S., Hattori, M., Kawada, E., Inoue, T., and Oda, Y. Control of bisphosphonate release using hydroxyapatite granules. *Journal of Biomedical Materials Research Part B: Applied Biomaterials*, 78B (2), 215–221 (2006).

[30] Garai, S., and Sinha, A. Biomimetic nanocomposites of carboxymethyl cellulose-hydroxyapatite: Novel three dimensional load bearing bone grafts. *Colloids and Surfaces B: Biointerfaces*, 115, 182–190 (2014).

[31] Liu, H., Cheng, J., Chen, F., Bai, D., Shao, C., Wang, J., Xi, P., and Zeng, Z. Gelatin functionalized graphene oxide for mineralization of hydroxyapatite: Biomimetic and in vitro evaluation. *Nanoscale*, 6 (10), 5315–5322 (2014).

[32] Liu, H., Cheng, J., Chen, F., Hou, F., Bai, D., Xi, P., and Zeng, Z. Biomimetic and cell-mediated mineralization of hydroxyapatite by carrageenan functionalized graphene oxide. *ACS Applied Materials and Interfaces*, 6 (5), 3132–3140 (2014).

[33] Depan, D., Pesacreta, T.C., and Misra, R.D.K. The synergistic effect of a hybrid graphene oxide-chitosan system and biomimetic mineralization on osteoblast functions. *Biomaterials Science*, 2 (2), 264–274 (2014).

[34] Mizushima, Y., Ikoma, T., Tanaka, J., Hoshi, K., Ishihara, T., Ogawa, Y., and Ueno, A. Injectable porous hydroxyapatite microparticles as a new carrier for protein and lipophilic drugs. *Journal of Controlled Release*, 110 (2), 260–265 (2006).

[35] Ahangari, M., Johar, M.H., and Saremi, M. Hydroxyapatite-carboxymethyl cellulose-graphene composite coating development on AZ31 magnesium alloy: Corrosion behavior and mechanical properties. *Ceramics International*, 47 (3), 3529–3539 (2021).

[36] Hummers, W.S., and Offeman, R.E. Preparation of Graphitic Oxide. *Journal of the American Chemical Society*, 80 (6), 1339 (1958).

[37] Li, M., Wang, Y., Liu, Q., Li, Q., Cheng, Y., Zheng, Y., Xi, T., and Wei, S. In situ synthesis and biocompatibility of nano hydroxyapatite on pristine and chitosan functionalized graphene oxide. *Journal of Materials Chemistry B*, 1 (4), 475–484 (2013).

[38] Hashem, M., Sharaf, S., Abd El-Hady, M.M., and Hebeish, A. Synthesis and characterization of novel carboxymethylcellulose hydrogels and carboxymethylcellulolse-hydrogel-ZnO-nanocomposites. *Carbohydrate Polymers*, 95 (1), 421–427 (2013).

[39] Li, W., Sun, B., and Wu, P. Study on hydrogen bonds of carboxymethyl cellulose

sodium film with two-dimensional correlation infrared spectroscopy. *Carbohydrate Polymers*, 78 (3), 454–461 (2009).

[40] Bricha, M., Belmamouni, Y., Essassi, E.M., Ferreira, J.M.F., and Mabrouk, K.E. Hydrothermal synthesis and appraisal of mg-doped hydroxyapatite nanopowders. *Journal of Biomaterials and Tissue Engineering*, 3 (5), 1–11 (2013).

[41] Ramani, D., and Sastry, T.P. Bacterial cellulose-reinforced hydroxyapatite functionalized graphene oxide: A potential osteoinductive composite. *Cellulose*, 21 (5), 3585–3595 (2014).

[42] Sumathra, M., Sadasivuni, K.K., Kumar, S.S., and Rajan, M. Cisplatin-Loaded Graphene Oxide/Chitosan/Hydroxyapatite Composite as a Promising Tool for Osteosarcoma-Affected Bone Regeneration. *ACS Omega*, 3 (11), 14620–14633 (2018).

[43] Bricha, M., Belmamouni, Y., Essassi, E.M., Ferreira, J.M.F., and El Mabrouk, K. Hydrothermal Synthesis and Appraisal of Mg-Doped Hydroxyapatite Nanopowders. *Journal of Biomaterials and Tissue Engineering*, 3 (5), 570–580 (2013).

[44] Belmamouni, Y., Bricha, M., Ferreira, J., and El Mabrouk, K. Hydrothermal synthesis of Si-doped hydroxyapatite nanopowders: Mechanical and bioactivity evaluation. *International Journal of Applied Ceramic Technology*, 12 (2), 329–340 (2015).

[45] Thomas, M., Naikoo, G.A., Sheikh, M.U.D., Bano, M., and Khan, F. Fabrication of hierarchically organized nanocomposites of Ba/alginate/carboxymethylcellulose/graphen e oxide/Au nanoparticles and their catalytic efficiency in o-nitroaniline reduction. *New Journal of Chemistry*, 39 (12), 9761–9771 (2015).

[46] Chen, F.F., Zhu, Y.J., Chen, F., Dong, L.Y., Yang, R.L., and Xiong, Z.C. Fire Alarm Wallpaper Based on Fire-Resistant Hydroxyapatite Nanowire Inorganic Paper and Graphene Oxide Thermosensitive Sensor. *ACS Nano*, 12 (4), 3159–3171 (2018).

[47] Peng, H., Meng, L., Niu, L., and Lu, Q. Simultaneous reduction and surface functionalization of graphene oxide by natural cellulose with the assistance of the ionic liquid. *Journal of Physical Chemistry C*, 116 (30), 16294–16299 (2012).

[48] Liu, A., and Berglund, L.A. Fire-retardant and ductile clay nanopaper biocomposites based on montmorrilonite in matrix of cellulose nanofibers and carboxymethyl cellulose. *European Polymer Journal*, 49 (4), 940–949 (2013).

[49] Biswal, D.R., and Singh, R.P. Characterisation of carboxymethyl cellulose and polyacrylamide graft copolymer. *Carbohydrate Polymers*, 57 (4), 379–387 (2004).

[50] Si, P., Si, P., and Si, P. POL YM ER M A T ER I PPy S i. 1997–1999 (2006).

[51] Salarian, M., Xu, W.Z., Wang, Z., Sham, T.K., and Charpentier, P.A. Hydroxyapatite-TiO2-based Nanocomposites Synthesized in Supercritical CO2for Bone Tissue Engineering: Physical and Mechanical Properties. *ACS Applied Materials and Interfaces*, 6 (19), 16918–16931 (2014).

[52] Türk, S., Altınsoy, I., Efe, G.Ç., Ipek, M., Özacar, M., and Bindal, C. The effect of reduction of graphene oxide on the formation of hydroxyapatite and tricalcium phosphate. *Vacuum*, 148, 1–10 (2018).

[53] Bao, H., Li, L., Gan, L.H., Ping, Y., Li, J., and Ravi, P. Thermo-and pH-responsive association behavior of dual hydrophilic graft chitosan terpolymer synthesized via ATRP and click chemistry. *Macromolecules*, 43 (13), 5679–5687 (2010).

[54] Tulain, U.R., Ahmad, M., Rashid, A., and Iqbal, F.M. Development and characterization of smart drug delivery system. *Acta Poloniae Pharmaceutica - Drug Research*, 73 (4), 1009–1022 (2016).

[55] Zhang, J., Wang, Q., and Wang, A. In situ generation of sodium alginate/hydroxyapatite nanocomposite beads as drug-controlled release matrices. *Acta Biomaterialia*, 6 (2), 445–454 (2010).

[56] Wang, H., Sun, D., Zhao, N., Yang, X., Shi, Y., Li, J., Su, Z., and Wei, G. Thermo-sensitive graphene oxide-polymer nanoparticle hybrids: Synthesis, characterization, biocompatibility and drug delivery. *Journal of Materials Chemistry B*, 2 (10), 1362–1370 (2014).

[57] Saldías, C., Velásquez, L., Quezada, C., and Leiva, A. Physicochemical assessment of Dextran-g-Poly (ε-caprolactone) micellar nanoaggregates as drug nanocarriers. *Carbohydrate Polymers*, 117, 458–467 (2015).

[58] Ritger, P.L., and Peppas, N.A. A simple equation for description of solute release I. Fickian and non-fickian release from non-swellable devices in the form of slabs, spheres, cylinders or discs. *Journal of Controlled Release*, 5 (1), 23–36 (1987).

[59] KOPCHA, M., LORDI, N.G., and TOJO, K.J. Evaluation of Release from Selected Thermosoftening Vehicles. *Journal of Pharmacy and Pharmacology*, 43 (6), 382–387 (1991).

[60] Korsmeyer, R.W., Gurny, R., Doelker, E., Buri, P., and Peppas, N.A. Mechanisms of solute release from porous hydrophilic polymers. *International Journal of Pharmaceutics*, 15 (1), 25–35 (1983).